Eur. Phys. J. C 17, 83–95 (2000)
Digital Object Identifier (DOI) 10.1007/s100520000465

THE EUROPEAN PHYSICAL JOURNAL C

Measurement of spin observables in neutron-proton elastic scattering

Part II: Rescattering parameters

J. Arnold[2], B. van den Brandt[3], M. Daum[3], Ph. Demierre[1], M. Finger[4,5], M. Finger,Jr.[5], J. Franz[2], N. Goujon-Naef[1], P. Hautle[3], R. Hess[1,a], A. Janata[5], J.A. Konter[3], H. Lacker[2], C. Lechanoine-Leluc[1], F. Lehar[6], S. Mango[3], D. Rapin[1], E. Rössle[2], P.A. Schmelzbach[3], H. Schmitt[2], P. Sereni[2], M. Slunečka[4,5], A. Teglia[1,3], B. Vuaridel[1]

[1] DPNC, Université de Genève, 1211 Genève 4, Switzerland
[2] Fakultät für Physik der Universität Freiburg, 79104 Freiburg, Germany
[3] PSI, Paul-Scherrer-Institut, 5232 Villigen-PSI, Switzerland
[4] MFF, Karlova Universita, 18000 Praha, Czech Republic
[5] LNP, Joint Institute for Nuclear Research, 141980 Dubna, Russia
[6] DAPNIA/SPP, CEA/Saclay, 91191 Gif-sur-Yvette (CEDEX) France

Received: 24 May 2000 / Published online: 31 August 2000 – © Springer-Verlag 2000

Abstract. A double scattering experiment, performed at the Paul-Scherrer-Institut (PSI), has measured a large variety of spin observables for free np elastic scattering from 260 to 535 MeV in the c.m. angle range from 60° to 164°. Results are presented for the depolarization parameters D_{onon}, $D_{os''os}$ and $D_{os''ok}$, the polarization transfer parameters K_{onno}, $K_{os''so}$ and $K_{os''ko}$, and the 3-index parameters N_{onkk}, $N_{os''kn}$, $N_{os''sn}$ and $N_{os''ns}$. The last four parameters have been measured for the first time in this energy range. These measurements considerably improve the data base available for neutron-proton scattering and will allow a direct reconstruction of the $I = 0$ scattering matrix, providing complete information about the nucleon-nucleon interaction in a model-independent way.

1 Introduction

This paper describes the measurement of the spin observables in np elastic scattering for which a measurement of the recoil proton polarization is required. It complements our measurements of spin correlation parameters performed with the same experimental apparatus [1]. This experiment was the basis of a Ph.D. thesis [2], where additional details may be found. All these measurements as well as those reported in [3] are part of the same neutron-proton scattering project at PSI.

The general method to measure the polarization of a particle requires an interaction which depends on the polarization to be analyzed. For the determination of the polarization in our experiment we used the scattering of the outgoing protons on carbon nuclei. The combination of the first scattering with the analyzing reaction is called a double scattering experiment. The definition of the axes used in the double scattering is given in Fig. 1 and the formalism used in this paper is given in [4].

The differential cross section for the analyzing reaction of a spin 1/2 particle with polarization $\mathbf{P}$ on an unpolarized target (carbon) has the form

$$\left(\frac{d\sigma}{d\Omega}\right)_C = I_C\ (1 + (\mathbf{P}\cdot\hat{n}_C\ )A_C\ ) \tag{1}$$

where I_C is the unpolarized differential cross section and $\hat{n}_C$ the normal to the scattering plane. The analyzing power A_C is a parameter depending on target material and thickness, scattering angle θ_C and reaction energy. The subscript C will always refer to the scattering on carbon.

The polarization vector is referred to the basis vectors of the recoil particle, $\hat{s}''$, $\hat{k}''$ and $\hat{n}$ as shown in Fig. 1. If ϕ_C is the angle between $\hat{n}$, the normal to the first scattering plane, and $\hat{n}_C$, the normal to the carbon scattering plane, we can decompose $\mathbf{P}$ on the three axes $\hat{s}'', \hat{n}, \hat{k}''$

$$\begin{aligned}\mathbf{P}\cdot\hat{n}_C &= P_n(\hat{n}\cdot\hat{n}_C) + P_{s''}(\hat{s}''\cdot\hat{n}_C) + P_{k''}\underbrace{(\hat{k}''\cdot\hat{n}_C)}_{=0},\\ &= P_n\cos\phi_C - P_{s''}\sin\phi_C.\end{aligned} \tag{2}$$

The longitudinal polarization cannot be analyzed since $\hat{n}_C$ is orthogonal to $\hat{k}''$. In order to observe this component it would be necessary to use a magnetic field in front of the analyzer to rotate the polarization. In the absence of such a magnetic field, all k'' components of the polarization tensor give no asymmetries in the measured dis-

[a] Deceased

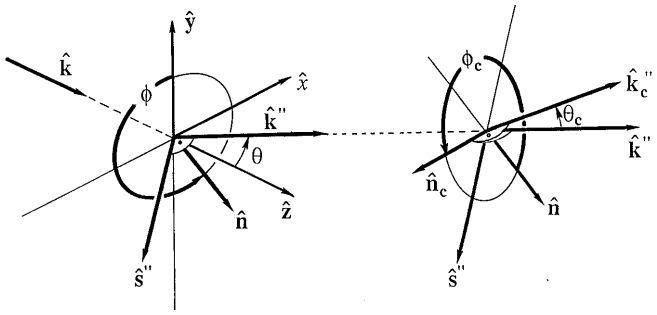

Fig. 1. Definition of angles in the first and second scattering

tribution. The differential cross section has the azimuthal dependence

$$\left(\frac{d\sigma}{d\Omega}\right)_C = I_C \ \{1 \underbrace{+A_C P_n}_{\epsilon_n} \cos\phi_C \underbrace{-A_C P_{s''}}_{\epsilon_{s''}} \sin\phi_C\}. \quad (3)$$

The analysis of the azimuthal distribution of the reaction determines the asymmetries ϵ_n and $\epsilon_{s''}$ by means of which the polarization can be determined if the analyzing power is known.

The polarization of a scattered particle is a measurable quantity which can be calculated from the scattering matrix M. The expected value of the polarization along a certain direction δ is the expectation value of the operator σ_δ in the final state

$$P_\delta \ = \ \langle\sigma_\delta\rangle_f \ = \frac{\mathrm{Tr}(\rho_f\sigma_\delta)}{\mathrm{Tr}(\rho_f)} = \frac{\mathrm{Tr}(M\rho_i M^\dagger\sigma_\delta)}{\mathrm{Tr}(M\rho_i M^\dagger)}. \quad (4)$$

Expanding the density matrix ρ_i in terms of spin observables yields

$$P_\delta \ = \frac{(P_{o\delta oo} + P_{B\alpha}K_{o\delta\alpha o} + P_{T\beta}D_{o\delta o\beta} + P_{B\alpha}P_{T\beta}N_{o\delta\alpha\beta})}{(1 + P_{B\alpha}A_{oo\alpha o} + P_{T\beta}A_{ooo\beta} + P_{B\alpha}P_{T\beta}A_{oo\alpha\beta})} \quad (5)$$

A summation is implicit over the greek indices α and β, running over the directions $\hat{n}$, $\hat{s}$ and $\hat{k}$.

Thus, by measuring the transverse components P_n and $P_{s''}$ for different orientations of the initial polarizations $\mathbf{P}_B$ and $\mathbf{P}_T$, the determination of several 3-spin parameters $N_{o\delta\alpha\beta}$, the 2-spin depolarization parameters $D_{o\delta o\beta}$ and spin transfer parameters $K_{o\delta\alpha o}$, is possible. The 10 parameters presented in this paper are: D_{onon}, $D_{os''os}$, $D_{os''ok}$, $K_{os''ko}$, K_{onno}, $K_{os''so}$, N_{onkk}, $N_{os''kn}$, $N_{os''sn}$ and $N_{os''ns}$. Note that the denominator of (5) is the differential cross section of the first scattering; the knowledge of all spin correlation parameters $A_{oo\alpha\beta}$ [1] are then a prerequisite.

2 Experimental apparatus and data taking

General aspects of the experimental method have been described earlier [3,5,6]. A brief description is also available in [1] and a summary is presented below with emphasis on new aspects.

The experiment, installed on the NA2 beam line at PSI, took advantage of the intense polarized neutron beam produced in the charge exchange reaction C(**p**, **n**)X at 0° using a high intensity longitudinally polarized proton beam ($10\mu A$) [7]. This beam had unique features: a continuous energy; a polarization between 17.4% at 260 MeV and 44.7% above 535 MeV; an intensity of a few 10^6 **n** s^{-1} cm^{-2} at 13.735 m from the production target. The beam energy was measured by time-of-flight using the rf signal from the accelerator. The beam polarization was reversed every second.

A polarized proton target (PPT) with a volume of 100 cm^3 working in frozen spin mode was used. Polarization values between 60% and 90% have been achieved. Details about the PPT are given in [1] and [8].

Both the scattered neutron and the recoil proton were detected in coincidence. The neutron detector consisted of a hodoscope made of 11 horizontal plastic scintillator bars of size $8 \times 20 \times 130$ cm^3 each viewed by two XP2040 photomultipliers [9]. A polarimeter was used to detect the recoil proton and to measure its transverse polarization by rescattering on a carbon target, 5 cm or 7 cm thick, sandwiched between MWPCs. Three chambers were placed in front and four behind the secondary carbon target. Each chamber had two orthogonal sense wire planes, X and Y, made of 20 μm tungsten wires spaced 2 mm apart. The two planes were 18 mm apart.

Both the neutron detector and the polarimeter were installed on rotatable platforms. Two angular settings referred to as positions "A" and "B" were used for the measurements covering the c.m. angular range from 64° to 120°, and 100° to 160°, respectively.

The trigger had two levels of event selection logic. The first level made a very simple and fast decision based on hits in scintillators, allowing selection of the $np \to np$ scattering events. A hardware second-level trigger allowed rejection of events with an angle of second scattering less than 3°. This second-level trigger was needed since only a small fraction (∼5%) of the recoil protons scattered on the carbon analyzing target and A_C is small for small scattering angles.

A detailed description of the decision logic is given in [3]. The main advantage of the second level trigger was to allow rejection within 3 μs of the events with a rescattering angle in carbon smaller than 3°. This important feature allowed to collect high statistics within a reasonable amount of time. Without this fast hardware decision, it would have taken about 20 times longer to get the same statistical accuracy.

3 Off-line data analysis

The reconstruction of particle trajectories and kinematic quantities for the first scattering has been described in [1, 3]. Starting from the coordinates of hit points in the detectors and from time-of-flight measurements, we calculated for each accepted physical event: (i) the scattering angles of the recoil proton (θ_p, ϕ_p) and of the scattered neutron

$(\theta_n,\ \phi_n)$ and (ii) the kinetic energy of the incident neutron (E). In order to determine the true recoil angles of the proton at the target from the path observed in the spectrometer, it was necessary to correct for the deflection of the proton in the magnetic field of the PPT.

In this section we describe selection criteria for second scattering events, in particular the requirement on the geometrical acceptance.

3.1 Trajectories and scattering angles of re-scattered protons

According to the definitions in Fig. 1, scattering angles have been calculated as

$$\cos\theta_C = \hat{k}'' \cdot \hat{k}''_C \quad \cos\phi_C = \hat{n}_C \cdot \hat{n} \quad \sin\phi_C = -\hat{n}_C \cdot \hat{s}'' \quad (6)$$

where $\hat{n}$ and $\hat{n}_C$ are normals to the first and second scattering planes given by

$$\hat{n} = -\frac{\mathbf{k} \times \mathbf{k}''}{|\mathbf{k} \times \mathbf{k}''|} \quad \text{and} \quad \hat{n}_C = \frac{\mathbf{k}'' \times \mathbf{k}''_C}{|\mathbf{k}'' \times \mathbf{k}''_C|}. \quad (7)$$

The trajectories of the re-scattered protons were calculated using the coordinates of the hit wires in the four MWPCs behind the carbon plate. The coordinates have been corrected for chamber misalignments. The χ^2 per degree of freedom (DOF) of the linear fit was calculated to check the alignment; events with $\chi^2 > 2/DOF$ have been rejected.

During the off-line analysis, the cut on the hardware angle decision (see Sect. 2) was refined and events have been accepted with $5^\circ < \theta_C < 20^\circ$. This cut was justified by the fact that the carbon analyzing power drops rapidly to zero at small scattering angles. The contribution of these events to the measurements of the spin observables was small and their on-line exclusion allowed us to collect a larger amount of useful data.

3.2 Second-scattering vertex

The reconstructed trajectories of the protons in front of and behind the carbon plates were used to calculate the second-scattering vertex. In order to select good events, the distance of closest approach between the incident and scattered tracks was computed. All events with this distance larger than 4.5 mm were rejected. The scattering vertex was calculated as the middle point of this minimal distance. Events having the reconstructed vertex outside the carbon plate were rejected. This cut eliminated mainly events scattered from the counters or the MWPCs which had previously been accepted for the trajectory reconstruction.

We calculated the incident proton energy of the second scattering starting from the energy of the outgoing proton from the first scattering and taking into account energy losses from the PPT to the center of the carbon plate. A correction has been taken from a look-up table with entries depending on the initial energy and recoil proton angles.

3.3 Geometrical acceptance

The spin observable evaluation was based on the determination of scattering asymmetries. In our analysis, we used the weighted sums method [10] described in Sect. 4.1 as the asymmetry estimator. For this method, it is not necessary to know the detection system acceptance (which would require a Monte Carlo acceptance calculation). The only restriction on the acceptance function η was that it is symmetric about π in ϕ_C. This means that

$$\eta(\theta_C, \phi_C) = \eta(\theta_C, \phi_C + \pi). \quad (8)$$

This condition could easily be checked: events were kept only if the detection of the mirror event would have been possible. Events that did not satisfy this condition were less than 5% of the total. The accepted events had to satisfy the following conditions: 1) the recoil trajectory was within the acceptance of the MWPCs; 2) the trajectory of the mirror track (which has $\phi'_C = \phi_C + \pi$) also hit all chambers.

4 Spin observables extraction

The determination of 3-index observables requires the measurement of the outgoing proton polarization. This could be done by analyzing the angular distribution of the second scattering. The analysis method used here, called the weighted sums method, will be presented in this section.

4.1 Weighted sums method

The angular distribution of a spin 1/2 particle with polarization $\mathbf{P}$ after a scattering on an unpolarized nucleus is given by (3), where the asymmetries ϵ_n and $\epsilon_{s''}$ are simple functions of the target analyzing power A_C and of the transverse polarization components of the incident particle.

Knowing the analyzing power [11] and for a given energy of the recoil proton, we are interested in estimating directly P_n and $P_{s''}$. If the acceptance function has a symmetry period of 180° in ϕ_C (cf. Sect. 3.3), it can be shown [10] that

$$\begin{pmatrix} \sum\limits_{ev} A_C \cos\phi_C \\ \sum\limits_{ev} A_C \sin\phi_C \end{pmatrix} = \begin{pmatrix} \sum\limits_{ev} A_C^2 \cos^2\phi_C & \sum\limits_{ev} A_C^2 \sin\phi_C \cos\phi_C \\ \sum\limits_{ev} A_C^2 \sin\phi_C \cos\phi_C & \sum\limits_{ev} A_C^2 \sin^2\phi_C \end{pmatrix} \times \begin{pmatrix} P_n \\ -P_{s''} \end{pmatrix} \quad (9)$$

where the sums are carried out over all events and the analyzing power $A_C(\theta_C)$ behaves as a weight. No other information about the detection system is necessary, except the knowledge of the target analyzing power as a function of θ_C under the experimental conditions in use, i.e. the same inelasticity and the same angular resolution. In this way, corrections for the inelasticity and the angular resolution are no longer necessary since they have been included in the analyzing power.

In matrix form, (9) is

$$\mathbf{G} = \mathsf{F}\ \mathbf{P} \tag{10}$$

and

$$\mathbf{P} = \mathsf{F}^{-1}\ \mathbf{G}. \tag{11}$$

Since our estimator $\mathbf{P}$ is a vector, we use the matrix notation for errors. In the ideal case with no background, the covariance matrix $\mathsf{V}(\mathbf{P})$ can be calculated by $\mathsf{V}(\mathbf{P}) = \mathsf{F}^{-1}$.

The estimator given in (11) is very practical for the background treatment because the subtraction has to be applied directly to the accumulated sums, and not to the polarizations. For background data, the corresponding sums $\mathbf{G_b}$ and $\mathsf{F_b}$ can be evaluated, and subtracted from the total sums $\mathbf{G_t}$ and $\mathsf{F_t}$. Then

$$\mathbf{G} = \mathbf{G_t} - \kappa\mathbf{G_b} \qquad \text{and} \qquad \mathsf{F} = \mathsf{F_t} - \kappa\mathsf{F_b} \tag{12}$$

where κ is the normalisation factor obtained by matching the wings of the distributions of the neutron-proton opening angles for the data obtained with the PPT and the dummy target data (see Sect. 3.4 in [1]). In this case the covariance matrix becomes

$$\mathsf{V}(\mathbf{P}) = \mathsf{F}^{-1}\left[\mathsf{F_t} + \kappa^2\mathsf{F_b}\right]\mathsf{F}^{-1}. \tag{13}$$

4.2 Spin precession in a magnetic field

The analysis described in the previous section gives the transverse components P_n and $P_{s''}$ of the recoil proton polarization $\mathbf{P}$ for each bin $(E, \Theta_{c.m.})$. The second scattering measures the two components of $\mathbf{P}$ perpendicular to the direction $\hat{k}_a$ of the recoil particle. Without any magnetic field, this is equal to $\hat{k}''$. If one chooses two other axes $\hat{n}_a, \hat{s}_a$ perpendicular to $\hat{k}_a$, the second scattering distribution (cf. (1)) becomes

$$\begin{aligned} &1 + A_C\left[(\mathbf{P}\cdot\hat{s}_a)\hat{s}_a + (\mathbf{P}\cdot\hat{n}_a)\hat{n}_a + (\mathbf{P}\cdot\hat{k}_a)\hat{k}_a\right]\cdot\hat{n}_C \\ &\quad = 1 - A_C(\mathbf{P}\cdot\hat{s}_a)\sin\phi_C + A_C(\mathbf{P}\cdot\hat{n}_a)\ \cos\phi_C, \end{aligned} \tag{14}$$

where $(\mathbf{P}\cdot\hat{s}_a)$ and $(\mathbf{P}\cdot\hat{n}_a)$ are the two components which can be measured. There is some arbitrariness in the choice of $\hat{n}_a$ and $\hat{s}_a$; any direction perpendicular to $\hat{k}_a$ is convenient. Without magnetic field in the PPT, $\hat{k}_a$ is identical to $\hat{k}''$ and it is natural to choose $(\hat{n}_a \equiv \hat{n})$, $(\hat{s}_a \equiv \hat{s}'')$ and $P_{s''}$, P_n are measured.

In fact, the evaluation of this polarization is complicated due to the magnetic field of the polarized target. During the passage through the magnetic field, both the trajectory and the polarization of the recoil proton are rotated, but not by the same amount due the anomalous magnetic moment. What we actually measure is then a "rotated" polarization $\mathbf{P}_R$. The trajectory direction $\hat{k}''$ is rotated to $\hat{k}''_{traj}(\equiv \hat{k}_a)$ and for the polarization analysis, the three axes $(\hat{s}'', \hat{n}, \hat{k}'')$ become $(\hat{s}''_R, \hat{n}_R, \hat{k}''_R \neq \hat{k}_a)$ after spin rotation. The two measured transverse components of the polarization are

$$\begin{aligned} P_{Rn} &= \mathbf{P}_R\cdot\hat{n}_a \\ &= P_n\ (\hat{n}_R\cdot\hat{n}_a) + P_{s''}\ (\hat{s}''_R\cdot\hat{n}_a) + P_{k''}\ (\hat{k}''_R\cdot\hat{n}_a) \end{aligned} \tag{15}$$

$$\begin{aligned} P_{Rs} &= \mathbf{P}_R\cdot\hat{s}_a \\ &= P_n\ (\hat{n}_R\cdot\hat{s}_a) + P_{s''}\ (\hat{s}''_R\cdot\hat{s}_a) + P_{k''}\ (\hat{k}''_R\cdot\hat{s}_a). \end{aligned} \tag{16}$$

We see that the final polarization has components along $\hat{n}, \hat{s}''$ and $\hat{k}''$. In our analysis, we have chosen to define $\hat{n}_a$ and $\hat{s}_a$ as

$$\hat{n}_a = -\frac{\mathbf{k}\times\mathbf{k}_a}{|\mathbf{k}\times\mathbf{k}_a|}, \quad \hat{s}_a = -\frac{\mathbf{n}_a\times\mathbf{k}_a}{|\mathbf{n}_a\times\mathbf{k}_a|}. \tag{17}$$

The rotations of the trajectory and spin are small because the holding field of the polarized frozen spin target is only 0.8 T and has a short field length. Therefore, the last two terms of ((15), (16)) are small. For either of the vertical or longitudinal holding field, these parasitic terms coming with k'' are smaller than 7%. The six scalar products have been calculated as analytical functions of the kinematic quantities of the reaction $(E, \Theta_{c.m.})$ taking into account the proton energy loss in the target.

4.3 Determination of spin parameters

The explicit forms of the measured P_{Rn} and P_{Rs} as functions of spin parameters and initial beam and target polarizations $(P_B,\ P_T)$ are combinations of the polarization components P_n, $P_{s''}$ and $P_{k''}$, which in turn can be expressed in terms of spin observables. One can write (5) explicitly as:

$$\begin{aligned} P_n = \mathcal{D}^{-1}(&P_{onoo} + P_{Bn}K_{onno} + P_{Tn}D_{onon} \\ &+P_{Bn}P_{Tn}N_{onnn} + P_{Bs}P_{Ts}N_{onss} + P_{Bk}P_{Tk}N_{onkk} \\ &+P_{Bs}P_{Tk}N_{onsk} + P_{Bk}P_{Ts}N_{onks}) \end{aligned} \tag{18}$$

$$\begin{aligned} P_{s''} = \mathcal{D}^{-1}(&P_{Bs}K_{os''so} + P_{Bk}K_{os''ko} + P_{Ts}D_{os''os} \\ &+P_{Tk}D_{os''ok} + P_{Bs}P_{Tn}N_{os''sn} + P_{Bn}P_{Ts}N_{os''ns} \\ &+P_{Bk}P_{Tn}N_{os''kn} + P_{Bn}P_{Tk}N_{os''nk}) \end{aligned} \tag{19}$$

$$\begin{aligned} P_{k''} = \mathcal{D}^{-1}(&P_{Bs}K_{ok''so} + P_{Bk}K_{ok''ko} + P_{Ts}D_{ok''os} \\ &+P_{Tk}D_{ok''ok} + P_{Bs}P_{Tn}N_{ok''sn} + P_{Bn}P_{Ts}N_{ok''ns} \\ &+P_{Bk}P_{Tn}N_{ok''kn} + P_{Bn}P_{Tk}N_{ok''nk}). \end{aligned} \tag{20}$$

The denominator $\mathcal{D}$ that all these expressions share is proportional to the differential cross section of the first scattering

$$\mathcal{D} = 1 + P_{Bn}A_{oono} + P_{Tn}A_{ooon} + \sum_{pq} P_{Bp}P_{Tq}A_{oopq}. \tag{21}$$

Table 1. Dominant parameters measured for different beam (P_B) and target (P_T) polarization orientations. For the data taken in position ($\mathbf{y}, \mathbf{xz}$), the target polarization was in the horizontal plane but turned by angle of $\alpha = 56.5°$. Therefore the measured parameters are linear combinations of pure spin observables, namely $D_{os''o\alpha}$= - $sin(\alpha)D_{os''os} + cos(\alpha)D_{os''ok}$ and $N_{os''n\alpha}$= - $sin(\alpha)N_{os''ns} + cos(\alpha)N_{os''nk}$. For details see [1]

P_B	P_T	Dominant parameters		
z	**z**	$D_{os''ok}$	$K_{os''ko}$	N_{onkk}
x	**y**	D_{onon}	$K_{os''so}$	$N_{os''sn}$
z	**y**	D_{onon}	$K_{os''ko}$	$N_{os''kn}$
y	**xz**	$D_{os''o\alpha}$	K_{onno}	$N_{os''n\alpha}$

If $\mathcal{D}$ is known (from previous measurements or from phase shift analyses predictions (PSA)), our attention can be focused on the 2- and 3-index parameters of the numerators and the extraction problem becomes linear. The two measured polarizations P_{Rn} and P_{Rs} are then linear combinations of 24 spin observables (O_α) explicitly given in (18–20) which can be written in vector mode as

$$\begin{aligned} P_{Rn} &= \sum_{\alpha=1}^{24} T^n_\alpha(E, \Theta_{c.m.}, \phi)\ O_\alpha(E, \Theta_{c.m.}) \\ P_{Rs} &= \sum_{\alpha=1}^{24} T^s_\alpha(E, \Theta_{c.m.}, \phi)\ O_\alpha(E, \Theta_{c.m.}) \\ &\rightarrow \quad \mathbf{P} = \sum_{\alpha=1}^{24} \mathbf{T}_\alpha(E, \Theta_{c.m.}, \phi)\ O_\alpha(E, \Theta_{c.m.}). \end{aligned} \tag{22}$$

The coefficients of these linear combinations $\mathbf{T}_\alpha(E, \Theta_{c.m.}, \phi)$, have been evaluated using the explicit ϕ-dependent form (see Fig. 1 for the definition of ϕ), expressing $\hat{s}$, $\hat{n}$, $\hat{k}$ and $\mathbf{P}_B$ and $\mathbf{P}_T$ in the laboratory frame $(\hat{x}, \hat{y}, \hat{z})$:

$$\begin{array}{l} \hat{s} = (\ \cos\phi,\ \sin\phi,\ 0\ ) \\ \hat{n} = (\ -\sin\phi,\ \cos\phi,\ 0\ ) \\ \hat{k} = (\ 0,\ 0,\ 1\ ) \end{array} \quad \text{and} \quad \begin{array}{l} \mathbf{P}_B = P_B(\ b_x,\ b_y,\ b_z\ ) \\ \mathbf{P}_T = P_T(\ t_x,\ t_y,\ t_z\ ). \end{array} \tag{23}$$

For instance, from (19), $N_{os''kn}$ has the coefficients

$$\begin{aligned} &T^n(E, \Theta_{c.m.}, \phi) \\ &\quad = \mathcal{D}^{-1}\ (\hat{s}''_R \cdot \hat{n}_a)\ P_{Bk}\ P_{Tn} \\ &\quad = \mathcal{D}^{-1}\ (\hat{s}''_R \cdot \hat{n}_a)\ P_B b_z\ P_T(t_y \cos\phi - t_x \sin\phi) \\ &T^s(E, \Theta_{c.m.}, \phi) \\ &\quad = \mathcal{D}^{-1}\ (\hat{s}''_R \cdot \hat{s}_a)\ P_{Bk}\ P_{Tn} \\ &\quad = \mathcal{D}^{-1}\ (\hat{s}''_R \cdot \hat{s}_a)\ P_B b_z\ P_T(t_y \cos\phi - t_x \sin\phi) \end{aligned} \tag{24}$$

in (15) and (16), respectively. Accepted events have been divided into energy and $\Theta_{c.m.}$, ϕ angle bins. Useful quantities were summed and recorded into sum-files. These energy-angle bins (refered as small bins) have been grouped in order to decrease statistical errors. Large bins have been obtained as follows: $\Theta_{c.m.}$ angle bins were combined yielding 8° wide bins; energy bins were grouped in order to have data at 5 energies with similar statistical errors and the five ϕ bins were grouped into a single bin. By grouping small bins, we also wanted to produce large groups centered at chosen nominal values ($E^0, \Theta^0_{c.m.}, \phi = 0$), allowing easier treatment and presentation of the results. A correction term has then been introduced in the following way:

$$\begin{aligned} &\sum_{\alpha=1}^{24} \mathbf{T}_\alpha(E^i, \Theta^i_{c.m.}, \phi_i)\ O_\alpha(E^i, \Theta^i_{c.m.}) \\ &\quad = \sum_{\alpha=1}^{24} \mathbf{T}_\alpha(E^i, \Theta^i_{c.m.},\ \phi_i)\ O_\alpha(E^0, \Theta^0_{c.m.}) \\ &\qquad + \sum_{\alpha=1}^{24} \mathbf{T}_\alpha(E^i, \Theta^i_{c.m.}, \phi_i) \\ &\qquad \times \underbrace{\left[O_\alpha(E^i, \Theta^i_{c.m.}) - O_\alpha(E^0, \Theta^0_{c.m.})\right]}_{\Delta O_{\alpha i}}, \end{aligned} \tag{25}$$

where now the parameters to be fitted are $O_\alpha(E^0, \Theta^0_{c.m.})$, and $\Delta O_{\alpha i}$ can be calculated using the observables predicted by the PSA [12]. The index i refers to a particular small bin.

For each large group we can then estimate the polarization vector $\mathbf{P}$ using (11), where $\mathsf{F} = \sum_i \mathsf{F}_i$ and $\mathbf{G} = \sum_i \mathbf{G}_i$. The final formula is then given as

$$\mathsf{F}^{-1}\mathbf{G} = \mathbf{P} = \sum_{\alpha=1}^{24} \langle \mathbf{T}_\alpha \rangle\ O_\alpha(E^0, \Theta^0_{c.m.}) + \langle \mathbf{C} \rangle \tag{26}$$

where coefficients and centering-corrections are the weighted average over the original small bins:

$$\begin{aligned} \langle \mathbf{T}_\alpha \rangle &= \mathsf{F}^{-1} \sum_i \mathsf{F}_i \mathbf{T}_{\alpha i} \qquad \text{and} \\ \langle \mathbf{C} \rangle &= \mathsf{F}^{-1} \sum_i \mathsf{F}_i \left(\sum_\alpha \mathbf{T}_{\alpha i} \Delta O_{\alpha i} \right). \end{aligned} \tag{27}$$

Measurements with various orientations of beam and target polarizations have been completed as indicated in Table 1, allowing a precise determination of the parameters that have, in turn, coefficient values close to 1. The dominant terms measured in each of the beam-target configurations are detailed in Table 1. One notices that D_{onon} is measured everytime the target is vertically polarized, and $K_{os''ko}$ everytime the beam is longitudinally polarized. One notices also that in the ($\mathbf{y}, \mathbf{xz}$) configuration one has measured a linear combination of two depolarization parameters and 3-index parameters due to the target polarization orientation. The fact that 3-index parameters always occur together with corresponding depolarization and spin transfer parameters and, moreover, the presence of parasitic terms, led us to estimate the observables by fitting the measurements for all the various beam/target polarization orientations simultaneously. Spin-parameters with small contributions to the recoil proton polarization could not be measured, therefore have been fixed to PSA prediction values [12].

Table 2. Relative uncertainty in the polarimeter analyzing power A_c. This is a scale uncertainty in all measured parameters involving rescattering on the carbon

$\Theta_{c.m.}$ [°]	260 MeV	315 MeV	380 MeV	460 MeV	535 MeV
64					6.9 %
72				5.4 %	3.4 %
80			5.4 %	3.0 %	1.6 %
88		6.2 %	3.4 %	1.6 %	1.5 %
96	8.1 %	4.2 %	1.8 %	1.5 %	1.5 %
104	5.9 %	2.8 %	1.5 %	1.5 %	1.5 %
112	4.3 %	1.7 %	1.5 %	1.5 %	1.5 %
120	3.2 %	1.5 %	1.5 %	1.5 %	1.5 %
128	2.2 %	1.5 %	1.5 %	1.5 %	1.5 %
136	1.7 %	1.5 %	1.5 %	1.5 %	1.5 %
144	1.5 %	1.5 %	1.5 %	1.5 %	1.5 %
152	1.5 %	1.5 %	1.5 %	1.5 %	1.5 %
60	1.5 %	1.5 %	1.5 %	1.5 %	1.5 %

Table 3. Relative errors of the beam polarization for the 5 energy bins. This is a scale error for all measured parameters

$260MeV$	$315MeV$	$380MeV$	$460MeV$	$535MeV$
2.4%	1.9%	1.9%	2.4%	2.1%

4.4 Systematic uncertainties

Multiplicative systematic errors are due to uncertainties in the determination factors of the observables involving the carbon analyzing power A_C, the beam polarization P_B and the target polarization P_T. These determination factors depend on the type of parameter measured; they are given by the products, $P_B A_C$, $P_T A_C$ and $P_T P_B A_C$ for the three types of measured parameters, namely $\mathrm{K}_{o\delta\alpha o}$, $\mathrm{D}_{o\delta o\beta}$ and $\mathrm{N}_{o\delta\alpha\beta}$, respectively.

In the determination of rescattering parameters, one always has the contribution of the carbon analyzing power, which has been measured [11] with an error mainly due to statistics and proton beam polarization uncertainty (both of the order of 1%). Analyzing power contributions to the measurement errors are given in Table 2. The relative error $\Delta A_C/A_C$ [11] is a function of the recoil proton energy. A constant value of 1.5% has been found, except for low energies and small c.m. scattering angles (corresponding to large proton laboratory angles). In these latter regions the relative error increases rapidly up to about 8%.

As described in [1,3], relative errors of the beam polarization are around 2%. They are given for the five neutron energy bins in Table 3. At low energies the uncertainty in the beam energy dominates.

The target polarization was measured with a relative precision between 3% and 4% [8] at 2.5 T in the high homogeneity solenoid before going into and after coming out of the frozen spin mode. Its value in the time in-between was calculated assuming an exponential decay. For data taken with a horizontally polarized target $(\hat{k}, \hat{s})$, an additional multiplicative uncertainty of $\pm 6\%$ has to be added as discussed in detail in [1].

Additive uncertainties on spin observables can be due to bias asymmetries in the experimental apparatus. Corrections have been applied for known and computable sources of systematic errors: misalignments of the proton polarimeter, energy and angular binning, asymmetry of the monitor used for normalisation. Uncertainties originating from the PSA values taken for the parasitic parameters were found to be negligible. Other possible additive biases can be due to the non-uniform efficiency of the MWPCs, residual misalignment and non-central passage through the polarimeter with asymmetric absorption and multiple scattering. Since we combined data with opposite target and/or beam spin orientations, these biases were effectively eliminated when extracting the parameters and are smaller than the statistical errors.

Our polarimeter has been optimized for a large angular acceptance and a high rescattering probability (thick carbon target); therefore it was well suited for measurements of 2- and 3-index parameters. On the other hand it was badly optimized for the measurement of P_{onoo} which could be affected by additive biases which could not be cancelled as discussed above because the sign of the physical effect could not be flipped. No results will therefore be given for P_{onoo}.

5 Results

We have measured six different 2-index parameters, D_{onon}, $D_{os''os}$, $D_{os''ok}$, K_{onno}, $K_{os''so}$, $K_{os''ko}$, and four three-index parameters, N_{onkk}, $N_{os''kn}$, $N_{os''sn}$, $N_{os''ns}$. The parameters requiring a sideway target polarization orientation (i.e $N_{os''ns}$ and $D_{os''os}$) have been measured as a linear combination of sideway (s) and longitudinal (k) parameters. The mixing of these two terms depended only

Table 4. Numerical values for D_{onon} as a function of $\Theta_{c.m.}$ and the neutron kinetic energy. "A" and "B" refer to the two overlapping angular positions. Errors are purely statistical

	$\Theta_{c.m.}$ [°]	260 MeV	315 MeV	380 MeV	460 MeV	535 MeV
	64				0.829 ± 0.098	0.795 ± 0.032
	72			0.727 ± 0.082	0.843 ± 0.034	0.870 ± 0.023
	80		0.865 ± 0.094	0.794 ± 0.032	0.901 ± 0.027	0.855 ± 0.023
"A"	88	0.783 ± 0.159	0.728 ± 0.032	0.762 ± 0.025	0.806 ± 0.026	0.839 ± 0.024
	96	0.448 ± 0.035	0.560 ± 0.021	0.668 ± 0.021	0.787 ± 0.026	0.787 ± 0.025
	104	0.220 ± 0.021	0.339 ± 0.017	0.498 ± 0.019	0.595 ± 0.025	0.649 ± 0.026
	112	0.021 ± 0.016	0.098 ± 0.015	0.221 ± 0.019	0.390 ± 0.026	0.417 ± 0.031
	120	-0.151 ± 0.045	-0.107 ± 0.045	0.036 ± 0.071	-0.121 ± 0.186	
	104	0.202 ± 0.035	0.291 ± 0.019	0.514 ± 0.022	0.564 ± 0.032	0.627 ± 0.038
	112	-0.043 ± 0.016	0.084 ± 0.013	0.206 ± 0.016	0.372 ± 0.022	0.419 ± 0.023
	120	-0.186 ± 0.012	-0.121 ± 0.012	-0.018 ± 0.015	0.090 ± 0.022	0.153 ± 0.024
"B"	128	-0.309 ± 0.011	-0.316 ± 0.011	-0.259 ± 0.014	-0.232 ± 0.021	-0.119 ± 0.023
	136	-0.392 ± 0.010	-0.422 ± 0.010	-0.437 ± 0.014	-0.426 ± 0.020	-0.397 ± 0.021
	144	-0.388 ± 0.010	-0.462 ± 0.011	-0.500 ± 0.014	-0.570 ± 0.018	-0.569 ± 0.020
	152	-0.262 ± 0.012	-0.377 ± 0.012	-0.501 ± 0.015	-0.572 ± 0.019	-0.651 ± 0.020
	160	-0.013 ± 0.023	-0.151 ± 0.023	-0.264 ± 0.031	-0.451 ± 0.040	-0.601 ± 0.046

Table 5. Numerical values for $D_{os''ok}$ as a function of $\Theta_{c.m.}$ and the neutron kinetic energy. "A" and "B" refer to the two overlapping angular positions. Errors are purely statistical

	$\Theta_{c.m.}$ [°]	260 MeV	315 MeV	380 MeV	460 MeV	535 MeV
	64				0.351 ± 0.148	0.497 ± 0.048
	72			0.168 ± 0.122	0.424 ± 0.050	0.531 ± 0.034
	80		0.149 ± 0.141	0.293 ± 0.047	0.456 ± 0.039	0.518 ± 0.032
"A"	88	0.131 ± 0.236	0.221 ± 0.046	0.407 ± 0.036	0.504 ± 0.036	0.499 ± 0.035
	96	0.294 ± 0.054	0.372 ± 0.031	0.412 ± 0.032	0.505 ± 0.037	0.608 ± 0.037
	104	0.221 ± 0.036	0.315 ± 0.025	0.356 ± 0.029	0.425 ± 0.036	0.530 ± 0.040
	112	0.268 ± 0.027	0.360 ± 0.022	0.408 ± 0.027	0.442 ± 0.036	0.543 ± 0.043
	120	0.285 ± 0.068	0.327 ± 0.053	0.351 ± 0.066	0.499 ± 0.106	0.459 ± 0.164
	104	0.279 ± 0.038	0.325 ± 0.020	0.380 ± 0.024	0.482 ± 0.035	0.530 ± 0.040
	112	0.284 ± 0.017	0.333 ± 0.014	0.396 ± 0.017	0.497 ± 0.023	0.471 ± 0.024
	120	0.261 ± 0.013	0.336 ± 0.012	0.386 ± 0.016	0.475 ± 0.022	0.445 ± 0.024
"B"	128	0.268 ± 0.011	0.294 ± 0.011	0.337 ± 0.015	0.333 ± 0.021	0.406 ± 0.023
	136	0.225 ± 0.011	0.254 ± 0.011	0.267 ± 0.014	0.271 ± 0.020	0.318 ± 0.021
	144	0.203 ± 0.011	0.220 ± 0.011	0.247 ± 0.014	0.257 ± 0.019	0.235 ± 0.020
	152	0.168 ± 0.013	0.168 ± 0.013	0.179 ± 0.015	0.179 ± 0.019	0.203 ± 0.020
	160	0.109 ± 0.023	0.124 ± 0.022	0.138 ± 0.027	0.092 ± 0.035	0.117 ± 0.038

Table 6. Numerical values for $D_{os''o\alpha}$ as a function of $\Theta_{c.m.}$ and the neutron kinetic energy. Its linear combination is given by: - 0.834 $D_{os''s}$ + 0.552 $D_{os''ok}$. "A" refers to the angular positions. Errors are purely statistical

	$\Theta_{c.m.}$ [°]	260 MeV	315 MeV	380 MeV	460 MeV	535 MeV
	64				0.990 ± 0.126	0.834 ± 0.038
	72			0.702 ± 0.100	0.910 ± 0.043	0.883 ± 0.028
	80		0.781 ± 0.114	0.856 ± 0.039	0.867 ± 0.034	0.900 ± 0.028
"A"	88	0.459 ± 0.195	0.652 ± 0.038	0.792 ± 0.030	0.802 ± 0.032	0.860 ± 0.029
	96	0.449 ± 0.043	0.543 ± 0.026	0.610 ± 0.025	0.724 ± 0.032	0.781 ± 0.031
	104	0.278 ± 0.026	0.411 ± 0.020	0.524 ± 0.023	0.591 ± 0.031	0.548 ± 0.031
	112	0.131 ± 0.020	0.247 ± 0.017	0.320 ± 0.021	0.353 ± 0.029	0.438 ± 0.033
	120	-0.011 ± 0.046	0.016 ± 0.039	0.096 ± 0.050	0.154 ± 0.084	0.005 ± 0.125

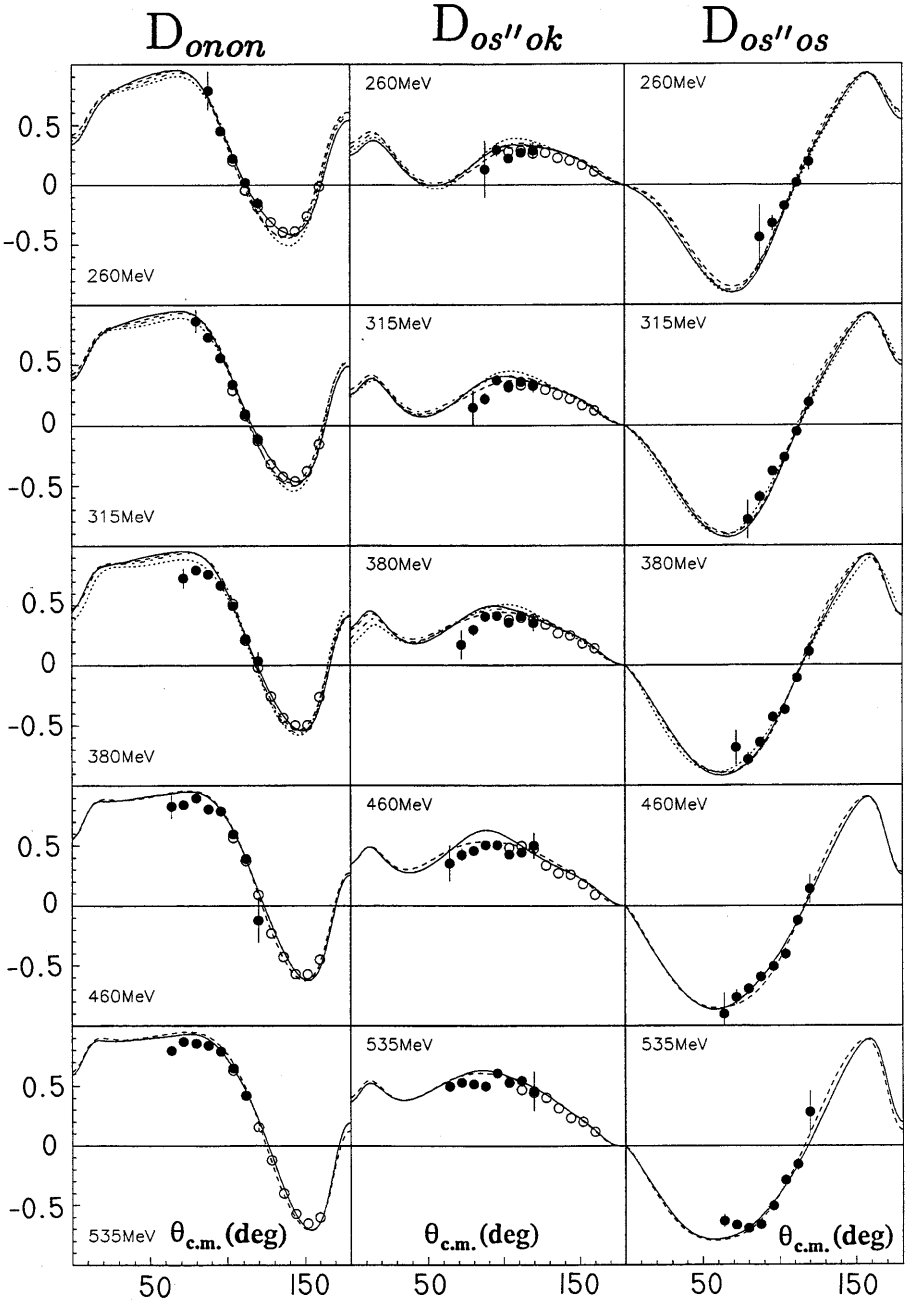

Fig. 2. Results for D_{onon}, $D_{os''os}$, $D_{os''ok}$ as function of $\Theta_{c.m.}$ and of the kinetic neutron energy. Black dots correspond to angular setting "A", open circles to position "B". Full line is a prediction from the PSA Saclay-Geneva [12], the dotted line from the Paris potential [14], the dashed line from VPI PSA [13] and the dashed-dotted line from the Bonn potential [16]

Table 7. Numerical values for K_{onno} as a function of $\Theta_{c.m.}$ and the neutron kinetic energy. "A" refer to the angular positions. Errors are purely statistical

	$\Theta_{c.m.}$ [°]	260 MeV	315 MeV	380 MeV	460 MeV	535 MeV
	64				-0.212 ± 0.228	-0.093 ± 0.057
	72			-0.044 ± 0.173	0.101 ± 0.072	-0.020 ± 0.044
	80		0.455 ± 0.283	0.204 ± 0.073	0.096 ± 0.058	0.024 ± 0.044
"A"	88	0.251 ± 0.686	0.151 ± 0.103	0.008 ± 0.056	-0.023 ± 0.052	0.144 ± 0.048
	96	0.331 ± 0.162	0.244 ± 0.071	-0.056 ± 0.049	-0.094 ± 0.052	0.100 ± 0.049
	104	-0.024 ± 0.103	-0.083 ± 0.057	-0.109 ± 0.045	-0.142 ± 0.050	-0.025 ± 0.050
	112	0.073 ± 0.077	-0.031 ± 0.048	-0.197 ± 0.041	-0.302 ± 0.047	-0.021 ± 0.053
	120	-0.050 ± 0.181	-0.176 ± 0.108	-0.060 ± 0.096	-0.136 ± 0.137	0.240 ± 0.211

Table 8. Numerical values for $K_{os''ko}$ as a function of $\Theta_{c.m.}$ and the neutron kinetic energy. "A" and "B" refer to the two overlapping angular positions. Errors are purely statistical

	$\Theta_{c.m.}$ [°]	260 MeV	315 MeV	380 MeV	460 MeV	535 MeV
	64				0.105 ± 0.310	0.103 ± 0.079
	72			-0.202 ± 0.230	-0.020 ± 0.100	-0.039 ± 0.060
	80		-0.135 ± 0.367	-0.159 ± 0.099	0.048 ± 0.079	0.182 ± 0.060
"A"	88		0.315 ± 0.131	0.160 ± 0.077	0.304 ± 0.074	0.250 ± 0.064
	96	0.617 ± 0.190	0.249 ± 0.091	0.188 ± 0.067	0.348 ± 0.074	0.325 ± 0.067
	104	0.007 ± 0.118	0.393 ± 0.073	0.417 ± 0.060	0.421 ± 0.069	0.210 ± 0.071
	112	0.266 ± 0.090	0.312 ± 0.063	0.341 ± 0.058	0.360 ± 0.074	0.473 ± 0.084
	120	0.063 ± 0.246	0.251 ± 0.186	0.234 ± 0.220		
	104	0.325 ± 0.152	0.406 ± 0.063	0.434 ± 0.051	0.367 ± 0.067	0.269 ± 0.071
	112	0.124 ± 0.072	0.329 ± 0.044	0.404 ± 0.037	0.382 ± 0.045	0.338 ± 0.043
	120	0.156 ± 0.055	0.201 ± 0.038	0.311 ± 0.034	0.414 ± 0.044	0.405 ± 0.044
"B"	128	0.105 ± 0.049	0.102 ± 0.036	0.187 ± 0.032	0.311 ± 0.042	0.342 ± 0.042
	136	-0.142 ± 0.046	0.046 ± 0.034	0.103 ± 0.031	0.146 ± 0.039	0.172 ± 0.039
	144	-0.061 ± 0.047	-0.074 ± 0.034	-0.121 ± 0.030	0.001 ± 0.037	0.113 ± 0.036
	152	-0.171 ± 0.055	-0.107 ± 0.040	-0.088 ± 0.034	-0.048 ± 0.039	0.077 ± 0.036
	160	-0.088 ± 0.101	-0.228 ± 0.073	-0.212 ± 0.066	-0.098 ± 0.077	-0.111 ± 0.081

Table 9. Numerical values for $K_{os''so}$ as a function of $\Theta_{c.m.}$ and the neutron kinetic energy. "A" and "B" refer to the two overlapping angular positions. Errors are purely statistical

	$\Theta_{c.m.}$ [°]	260 MeV	315 MeV	380 MeV	460 MeV	535 MeV
	64				-0.554 ± 0.288	-0.061 ± 0.072
	72			0.242 ± 0.210	-0.011 ± 0.088	-0.070 ± 0.053
	80		0.004 ± 0.346	0.245 ± 0.089	-0.163 ± 0.070	-0.086 ± 0.054
"A"	88		0.023 ± 0.129	0.213 ± 0.070	0.090 ± 0.065	0.014 ± 0.057
	96	0.023 ± 0.202	0.095 ± 0.089	0.261 ± 0.061	0.160 ± 0.066	-0.003 ± 0.060
	104	0.037 ± 0.127	0.129 ± 0.072	0.340 ± 0.056	0.113 ± 0.062	0.079 ± 0.063
	112	-0.208 ± 0.099	-0.010 ± 0.063	0.161 ± 0.055	0.199 ± 0.067	0.179 ± 0.074
	120	0.133 ± 0.278	-0.254 ± 0.195	0.091 ± 0.209		
	104	0.125 ± 0.227	-0.004 ± 0.092	0.195 ± 0.077	0.375 ± 0.099	0.196 ± 0.106
	112	-0.111 ± 0.110	0.109 ± 0.066	0.071 ± 0.055	0.041 ± 0.066	0.159 ± 0.064
	120	-0.138 ± 0.086	-0.036 ± 0.059	-0.003 ± 0.051	0.189 ± 0.066	0.227 ± 0.067
"B"	128	-0.343 ± 0.077	-0.251 ± 0.054	-0.074 ± 0.049	-0.041 ± 0.063	0.131 ± 0.064
	136	-0.388 ± 0.072	-0.389 ± 0.052	-0.283 ± 0.046	-0.190 ± 0.058	-0.047 ± 0.058
	144	-0.797 ± 0.074	-0.572 ± 0.052	-0.515 ± 0.046	-0.442 ± 0.055	-0.214 ± 0.053
	152	-0.891 ± 0.086	-0.666 ± 0.061	-0.755 ± 0.050	-0.685 ± 0.057	-0.494 ± 0.053
	160	-0.820 ± 0.157	-0.923 ± 0.108	-0.958 ± 0.102	-0.968 ± 0.119	-0.730 ± 0.125

Table 10. Numerical values for N_{onkk} as a function of $\Theta_{c.m.}$ and the neutron kinetic energy. "B" refers to the angular positions. Errors are purely statistical

	$\Theta_{c.m.}$ [°]	260 MeV	315 MeV	380 MeV	460 MeV	535 MeV
	104	-0.163 ± 0.436	-0.210 ± 0.174	-0.108 ± 0.137	-0.342 ± 0.170	-0.294 ± 0.179
	112	-0.352 ± 0.197	-0.231 ± 0.114	-0.251 ± 0.092	-0.333 ± 0.108	-0.501 ± 0.103
	120	-0.076 ± 0.147	-0.311 ± 0.098	-0.336 ± 0.085	-0.415 ± 0.102	-0.494 ± 0.103
"B"	128	0.021 ± 0.129	-0.216 ± 0.090	-0.198 ± 0.077	-0.563 ± 0.097	-0.319 ± 0.097
	136	-0.212 ± 0.122	-0.275 ± 0.086	-0.273 ± 0.074	-0.189 ± 0.091	-0.314 ± 0.090
	144	0.111 ± 0.125	-0.171 ± 0.086	-0.187 ± 0.074	-0.293 ± 0.090	-0.161 ± 0.084
	152	0.007 ± 0.143	-0.172 ± 0.101	-0.128 ± 0.083	-0.062 ± 0.094	-0.240 ± 0.087
	160	0.442 ± 0.246	-0.045 ± 0.172	0.007 ± 0.147	-0.013 ± 0.168	-0.163 ± 0.171

Table 11. Numerical values for $N_{os''kn}$ as a function of $\Theta_{c.m.}$ and the neutron kinetic energy. "A" and "B" refer to the two overlapping angular positions. Errors are purely statistical

	$\Theta_{c.m.}$ [°]	260 MeV	315 MeV	380 MeV	460 MeV	535 MeV
	64				-0.160 ± 0.443	0.071 ± 0.112
	72			-0.204 ± 0.335	-0.063 ± 0.144	0.124 ± 0.085
	80			0.030 ± 0.145	0.181 ± 0.114	0.128 ± 0.086
"A"	88		-0.189 ± 0.201	-0.100 ± 0.114	0.079 ± 0.108	0.295 ± 0.092
	96	0.095 ± 0.307	0.033 ± 0.141	0.108 ± 0.099	0.270 ± 0.107	0.236 ± 0.097
	104	0.171 ± 0.191	0.063 ± 0.112	-0.019 ± 0.089	0.295 ± 0.100	0.053 ± 0.103
	112	0.062 ± 0.148	0.043 ± 0.098	0.236 ± 0.086	0.221 ± 0.108	0.105 ± 0.122
	120	0.142 ± 0.422	0.137 ± 0.302	0.519 ± 0.341		
	104	0.000 ± 0.266	0.113 ± 0.112	-0.032 ± 0.092	0.161 ± 0.120	-0.013 ± 0.132
	112	0.175 ± 0.129	0.027 ± 0.079	0.092 ± 0.067	0.227 ± 0.084	0.374 ± 0.080
	120	0.238 ± 0.100	0.158 ± 0.070	0.197 ± 0.063	0.202 ± 0.082	0.096 ± 0.082
"B"	128	0.352 ± 0.089	0.108 ± 0.065	0.178 ± 0.060	0.232 ± 0.078	0.179 ± 0.079
	136	0.243 ± 0.084	0.315 ± 0.062	0.224 ± 0.057	0.138 ± 0.073	0.093 ± 0.072
	144	0.368 ± 0.085	0.375 ± 0.063	0.312 ± 0.056	0.222 ± 0.069	0.005 ± 0.066
	152	0.254 ± 0.100	0.170 ± 0.074	0.270 ± 0.062	0.074 ± 0.071	0.054 ± 0.067
	160	0.258 ± 0.186	0.112 ± 0.135	0.264 ± 0.127	0.020 ± 0.150	-0.136 ± 0.158

Table 12. Numerical values for $N_{os''n\alpha}$ as a function of $\Theta_{c.m.}$ and the neutron kinetic energy. Its linear combination is given by: - 0.834 $N_{os''ns}$ + 0.552 $N_{os''nk}$. "A" refers to the angular positions. Errors are purely statistical

	$\Theta_{c.m.}$ [°]	260 MeV	315 MeV	380 MeV	460 MeV	535 MeV
	64				-0.163 ± 0.317	0.154 ± 0.079
	72			-0.200 ± 0.235	-0.014 ± 0.100	-0.009 ± 0.060
	80		-0.271 ± 0.390	-0.082 ± 0.100	-0.085 ± 0.080	-0.055 ± 0.061
"A"	88		-0.149 ± 0.144	-0.006 ± 0.079	-0.146 ± 0.074	-0.128 ± 0.065
	96	0.221 ± 0.226	-0.112 ± 0.099	-0.172 ± 0.067	-0.256 ± 0.073	-0.280 ± 0.068
	104	0.075 ± 0.142	-0.164 ± 0.079	-0.322 ± 0.062	-0.191 ± 0.071	-0.280 ± 0.069
	112	-0.044 ± 0.107	-0.150 ± 0.067	-0.206 ± 0.057	-0.214 ± 0.067	-0.166 ± 0.074
	120	-0.406 ± 0.249	-0.124 ± 0.152	0.093 ± 0.135	-0.189 ± 0.190	-0.556 ± 0.290

Table 13. Numerical values for $N_{os''sn}$ as a function of $\Theta_{c.m.}$ and the neutron kinetic energy. "A" and "B" refer to the two overlapping angular positions. Errors are purely statistical

	$\Theta_{c.m.}$ [°]	260 MeV	315 MeV	380 MeV	460 MeV	535 MeV
	64				0.455 ± 0.401	-0.162 ± 0.100
	72			-0.180 ± 0.295	-0.348 ± 0.124	-0.173 ± 0.074
	80		-0.677 ± 0.492	-0.138 ± 0.126	-0.142 ± 0.098	-0.060 ± 0.076
"A"	88		0.059 ± 0.184	-0.085 ± 0.099	-0.047 ± 0.091	-0.143 ± 0.080
	96	-0.541 ± 0.296	-0.248 ± 0.128	-0.087 ± 0.087	-0.182 ± 0.094	0.019 ± 0.085
	104	-0.117 ± 0.186	0.058 ± 0.104	-0.191 ± 0.079	-0.124 ± 0.087	0.071 ± 0.090
	112	-0.186 ± 0.145	-0.052 ± 0.091	-0.096 ± 0.078	-0.228 ± 0.095	-0.185 ± 0.104
	120	0.221 ± 0.412	-0.223 ± 0.283	0.121 ± 0.300		
	104	-0.274 ± 0.334	-0.076 ± 0.134	-0.050 ± 0.112	-0.181 ± 0.143	0.170 ± 0.153
	112	-0.216 ± 0.162	0.092 ± 0.097	-0.106 ± 0.080	-0.132 ± 0.096	-0.036 ± 0.092
	120	-0.029 ± 0.127	-0.159 ± 0.086	-0.022 ± 0.075	-0.087 ± 0.095	-0.051 ± 0.097
"B"	128	-0.010 ± 0.113	0.075 ± 0.079	0.056 ± 0.071	0.038 ± 0.091	0.036 ± 0.092
	136	-0.005 ± 0.106	0.183 ± 0.075	-0.043 ± 0.067	-0.029 ± 0.084	-0.005 ± 0.083
	144	0.118 ± 0.108	0.050 ± 0.075	0.063 ± 0.066	0.052 ± 0.080	0.093 ± 0.077
	152	0.101 ± 0.127	0.129 ± 0.089	0.139 ± 0.072	0.178 ± 0.082	0.069 ± 0.077
	160	0.073 ± 0.232	0.073 ± 0.158	-0.196 ± 0.148	0.226 ± 0.171	-0.015 ± 0.180

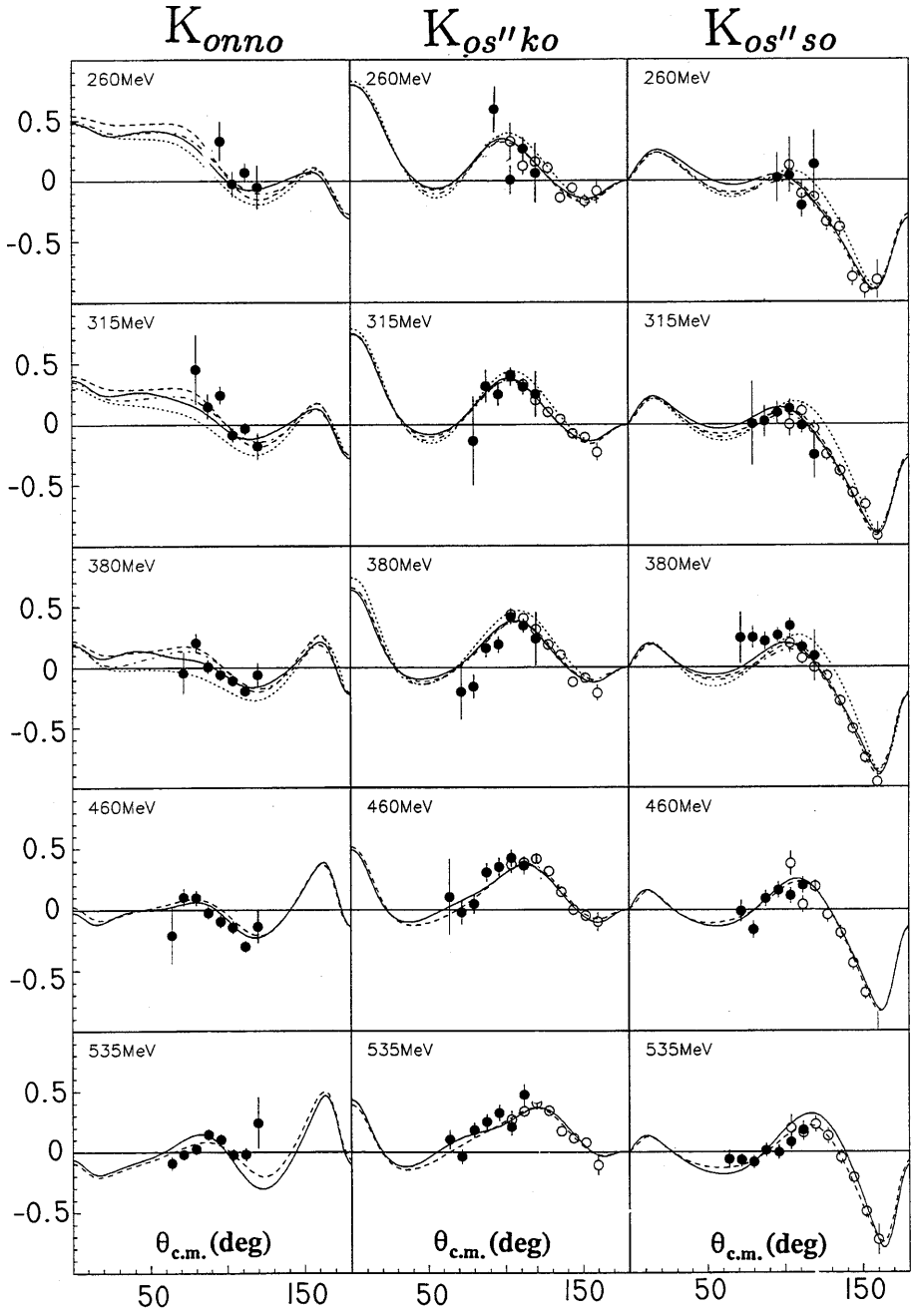

Fig. 3. Results for K_{onno}, $K_{os''so}$, $K_{os''ko}$ as function of $\Theta_{c.m.}$ and of the kinetic neutron energy. The same symbols are used as in Fig. 2

on the angle $\alpha = 56.5°$ by which the polarized target was turned with respect to the beam direction since all other small parasitic terms have been taken into account as discussed in Sect. 4.3. Therefore the measured observables are $D_{os''o\alpha}$= - $sin(\alpha)D_{os''os} + cos(\alpha)D_{os''ok}$ and $N_{os''n\alpha}$= - $sin(\alpha)N_{os''ns} + cos(\alpha)N_{os''nk}$.

Numerical values for the ten measured observables are given in Tables 4–13. The errors are purely statistical. Results are given as a function of the c.m. scattering angle ($\Theta_{c.m.}$) for five energies, namely 260, 315, 380, 460 and 535 MeV. These energies correspond to the central values of five energy bins covering the intervals 230-290, 290-340, 340-420, 420-500 and 500-570 MeV, respectively. The measured angular range was covered with two detector arm positions providing an overlapping angular region of about $10°_{c.m.}$. The 3-index parameter N_{onkk} was measured only in the "B" position and the parameters K_{onno}, $D_{os''o\alpha}$ and $N_{os''n\alpha}$ in the "A" position only. The corresponding results are plotted in Figs. 2 to 4 as dots (for position "A") and open circles (for position "B"). The overlapping points are in good agreement with each other. In the figures we have shown the pure parameters $D_{os''os}$ and $N_{os''ns}$ instead of the measured linear combinations to ease the comparison with theoretical predictions.

In each figure, four phenomenological predictions of spin observables are shown: solid and dashed lines correspond to the Saclay-Geneva phase shift analysis [12] and to the VPI PSA 1998 solution [13], respectively. The two

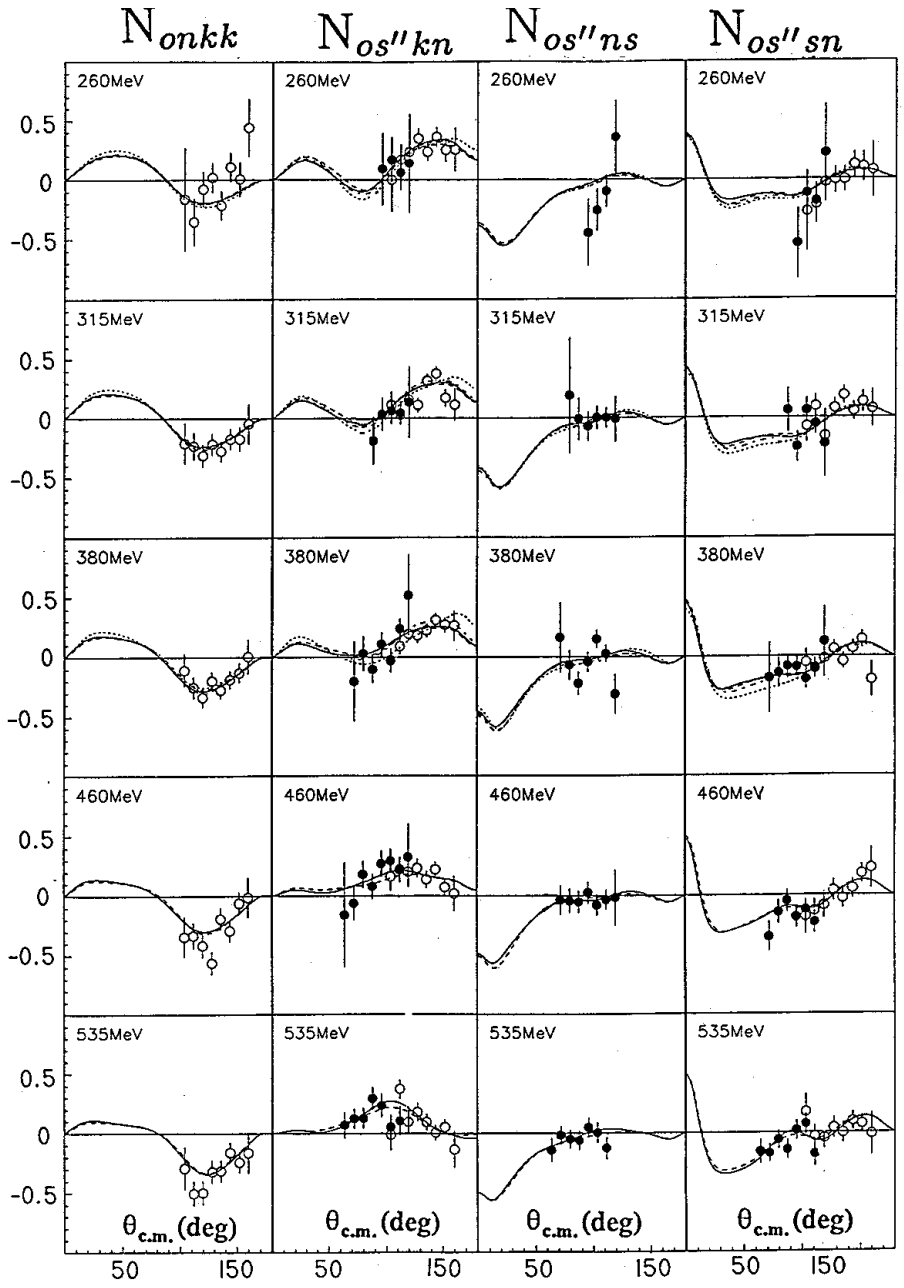

Fig. 4. Results for N_{onkk}, $N_{os''kn}$, $N_{os''ns}$, $N_{os''sn}$ as function of $\Theta_{c.m.}$ and of the kinetic neutron energy. The same symbols are used as in Fig. 2

other predictions were obtained from potential model calculations, the dotted line corresponds to the Paris potential [14] and the dash-dotted one to the Bonn potential [15,16]. All these predictions are in good agreement with each other, except for the two n index parameter K_{onno}. A similar disagreement has been observed for the two n index spin correlation parameter, A_{oonn}, in [1]. Even for the 3-index parameters, which had not been measured previously, the agreement is surprisingly good. Previous data on these ten spin parameters in this energy range [17-27] are summarized in Table 14. They are not plotted in the figures as they were measured at somewhat different energies. These data, mostly measured at TRIUMF [23-26], consist mainly of spin-transfer parameters obtained with a polarized beam and an unpolarized target. Neither the 3-index parameters nor $D_{os''os}$ and $D_{os"ok}$ parameters have been measured previously.

The present experiment has considerably improved the data available for neutron-proton scattering and will allow a future direct reconstruction of the scattering matrix. This large number of observables is necessary in order to remove ambiguities, since the amplitudes are extracted by solving simultaneously a set of quadratic equations. In practice, the over-determination of the system is of much greater importance than a high precision of the data, which is anyway limited by systematic uncertainties.

Table 14. Available data for the depolarization and polarization-transfer parameters in the energy range 200-600 MeV. The asterik (*) denotes $p-n$ experiments

	lab [ref]	energy	points	angular range	typical errors
D_{onon}	Rochester '62 [20] (*)	212 MeV	5	40° - 80°	0.17
	Chicago '68 [19] (*)	425 MeV	3	44° - 90°	0.03
	Gatchina '81 [18]	600 MeV	4	130° - 160°	0.12
	LAMPF '86 [17]	496 MeV	3	22° - 44°	0.07
K_{onno}	TRIUMF '77 [25]	516 MeV	3	153° - 166°	0.07
	TRIUMF '80 [23]	220 MeV	10	98° - 152°	0.08
		325 MeV	12	84° - 152°	0.06
		425 MeV	16	66° - 158°	0.07
		495 MeV	17	60° - 158°	0.10
	LAMPF '93 [21]	485 MeV	30	60° - 160°	0.07
$K_{os''so}$	Berkeley '70 [22]	520 MeV	3	90° - 124°	0.16
		600 MeV	3	65° - 102°	0.17
	TRIUMF '77 [25]	343 MeV	4	141° - 167°	0.19
		516 MeV	3	153° - 167°	0.09
	TRIUMF '80 [24]	220 MeV	7	97° - 152°	0.07
		325 MeV	9	77° - 153°	0.05
		425 MeV	11	67° - 163°	0.07
		495 MeV	11	65° - 163°	0.07
	TRIUMF '89 [26]	228 MeV	1	160°	0.03
		337 MeV	1	160°	0.03
		440 MeV	1	160°	0.03
	LAMPF '92 [27]	485 MeV	5	114° - 176°	0.04
$K_{os''ko}$	TRIUMF '80 [24]	220 MeV	7	97° - 152°	0.09
		325 MeV	8	77° - 144°	0.05
		425 MeV	11	67° - 163°	0.07
		495 MeV	11	65° - 163°	0.07
	LAMPF '92 [27]	485 MeV	7	74° - 176°	0.04

Our measured data will be useful for stabilizing phase shift predictions and should encourage theoreticians to improve their model for a better description of the data.

Acknowledgements. We thank the Paul-Scherrer-Institute for its valuable technical assistance. Thanks are also due to P. Extermann for his continuous support and encouragement during the course of this experiment. Many useful discussions with L.G. Greeniaus are hereby acknowledged. We also would like to thank the technical staff of the University of Geneva. This work was supported by the Fonds National Suisse and the German BMBF.

References

1. J. Arnold et al., see the same issue of Eur. Phys. J. C
2. A. Teglia, PhD thesis, Univ. of Geneva (1997) No. 2948
3. A. Ahmidouch, et al., Eur. Phys. J. C **2**, 627 (1998)
4. J. Bystricky, F. Lehar and P.Winternitz, J. Phys. (Paris) **39**, 1 (1978)
5. J. Arnold et al., Nucl. Instrum. Methods A **386**, 211 (1997)
6. J. Arnold et al., Eur. Phys. J. A **2**, 411 (1998)
7. R. Binz et al. Phys. Lett. B **231**, 323 (1989)
8. B. van den Brandt et al. Nucl. Instrum. Methods A **356**, 53 (1995)
9. A. Ahmidouch et al., Nucl. Instrum. Methods A **326**, 538 (1993)
10. D. Besset et al., Nucl. Instrum. Methods **166**, 515 (1979)
11. E. Aprile-Giboni et al., Nucl. Instrum. Methods **215**, 147 (1983)
12. J. Bystricky et al., J. Phys. (France) **48**, 199 (1987)
13. R.A. Arndt et al., SAID - Scattering Analyses Interactive Dial-In, www-address: http://clsaid.phys.vt.edu/~CAPS/
14. M. Lacombe et al., Phys. Rev. D **12**, 1495 (1975) and Phys. Rev. C **21**, 861 (1988)
15. R. Machleidt et al., Phys. Rept. **149**, 1 (1987)
16. C. Elster, et al., Phys. Rev. C **37**, 1647 (1988) and Phys. Rev. C **38**, 1828 (1988)
17. J.A. Marshall et al., Phys. Rev. C **34**, 1433 (1986)
18. Yu.Sh. Bagaturiya, et al., Sov.J.Nucl.Phys. 33, 659 (1981)
19. S.C. Wright, et al., Phys. Rev. **175**, 1704 (1968)
20. R.E. Warner, et al., Phys. Rev. C **34**, 1433 (1986)
21. M.W. McNaughton, et al., Phys. Rev. C **48**, 256 (1993)
22. Kwok-chu Leung, PhD thesis, UCRL-19705 (1970)
23. A.S. Clough, et al., Phys. Rev. C **21**, 988 (1980)
24. D. Axen, et al., Phys. Rev. C **21**, 988 (1980)
25. C. Amsler, et al., Nucl. Instrum. Methods **144**, 401 (1977)
26. D. Bandyopadhyay, et al., Phys. Rev. C **40**, 2684 (1989)
27. K.H. McNaughton, et al., Phys. Rev. C **46**, 47 (1992)